



Natural sea-salt emissions moderate the climate forcing of anthropogenic nitrate

Ying Chen^{1,2,3,8,*}, Yafang Cheng^{2,*}, Nan Ma^{4,2,3,1}, Chao Wei³, Liang Ran⁵, Ralf Wolke¹, Johannes Größl¹, Qiaoqiao Wang⁴, Andrea Pozzer⁶, Hugo A. C. Denier van der Gon⁷, Gerald Spindler¹, Jos Lelieveld^{6,9}, Ina Tegen¹, Hang Su³, Alfred Wiedensohler¹

¹Leibniz-Institute for Tropospheric Research, Leipzig, Germany

²Minerva Research Group, Max Planck Institute for Chemistry, Mainz, Germany

³Multiphase Chemistry Department, Max Planck Institute for Chemistry, Mainz, Germany

⁴Center for Pollution and Climate Change Research (APCC), Institute for Environmental and Climate Research, Jinan University, Guangzhou, China

⁵Key Laboratory of Middle Atmosphere and Global Environment Observation, Institute of Atmospheric Physics, Chinese Academy of Sciences, Beijing, China

⁶Atmospheric Chemistry Department, Max Planck Institute for Chemistry, Mainz, Germany

⁷TNO, Dept. of Climate, Air and Sustainability, Princetonlaan 6, Utrecht, the Netherlands

⁸Lancaster Environment Centre, Lancaster University, Lancaster, UK

⁹The Cyprus Institute, Nicosia, Cyprus

*Correspondence to: yafang.cheng@mpic.de (Y.F.C.); chen@tropos.de (Y.C.)

20

Abstract. Natural sea-salt aerosols, when interacting with anthropogenic emissions, can enhance the formation of particulate nitrate. This enhancement has been suggested to increase the direct radiative forcing of nitrate, called ‘mass-enhancement effect’. Through a size-resolved dynamic mass transfer modelling approach, we show that interactions with sea-salt shift the nitrate from sub- to super-micron sized particles (‘re-distribution effect’), and hence lower its efficiency for light extinction and reduce its lifetime. The re-distribution effect overwhelms the mass-enhancement effect and significantly moderates nitrate cooling; e.g., the nitrate associated aerosol optical depth can be reduced by 10-20% over European polluted regions during a typical sea-salt event, in contrast to an increase by ~10% when only accounting for the mass-enhancement effect. Global model simulations indicate significant re-distribution over coastal and offshore regions world-wide. Our study suggests a strong buffering by natural sea-salt aerosols that reduces the climate forcing of anthropogenic nitrate, which had been expected to dominate the aerosol cooling by the end of the century. Comprehensive considerations of this re-distribution effect foster better understandings of climate change and nitrogen deposition.

25

30



1. Introduction

35 Particulate nitrate (NO_3^-) is one of the most important anthropogenic aerosol components that exert a climate cooling effect (IPCC, 2013; Haywood and Schulz, 2007). On a global scale, its average direct radiative forcing (DRF) has been estimated to span over a relatively wide range from -0.08 to -0.19 W m^{-2} (Liao et al., 2004; Liao and Seinfeld, 2005; IPCC, 2013; Xu and Penner, 2012; Haywood and Schulz, 2007; Myhre et al., 2013; Forster et al., 2007; Adams et al., 2001; Bauer et al., 2007; Jacobson, 2001; Streets et al., 2013; van Dorland et al., 1997). It is projected to reach up to about -0.4 to -1.3 W m^{-2} and dominate the aerosol cooling by the end of the century (Adams et al., 2001; Bellouin et al., 2011; Hauglustaine et al., 2014). Although the gaseous precursors of nitrate, e.g., NO_x ($= \text{NO} + \text{NO}_2$) and HNO_3 , are mainly of anthropogenic origin, globally about 35-50% of the nitrate mass is associated with natural sea-salt aerosol (Xu and Penner, 2012; Myhre et al., 2006). This is because sea-salt aerosol can be transported over industrialized regions, 45 interacts with anthropogenic precursors of nitrate and enhances the total nitrate column loading in the atmosphere through heterogeneous uptake of HNO_3 and its precursors (Liao et al., 2004; Liao and Seinfeld, 2005; Seinfeld and Pandis, 2006; Xu and Penner, 2012; Ravishankara, 1997; Lowe et al., 2015). Such sea-salt-induced nitrate mass increase is believed to strengthen the DRF and climate cooling of nitrate (Liao and Seinfeld, 2005), called the ‘mass-enhancement effect’.

50 However, not only the mass concentration but also the particle mass size distribution (PMSD) are essential for evaluating the direct radiative forcing of nitrate ($\text{DRF}_{\text{nitrate}}$) (IPCC, 2013; Murphy et al., 1998; Kok et al., 2017). Besides leading to the increase of total nitrate mass, interactions with sea-salt aerosol also have a ‘re-distribution effect’ on nitrate PMSD which shifts nitrate from sub- to super-micron sizes (e.g., Chen et al., 2016a, see also Fig. 1). Because sea-salt aerosol is mainly present as super-micron (coarse) 55 particles (Murphy et al., 1998; O’Dowd et al., 1997; Ravishankara, 1997), chemical equilibrium favors the formation of thermodynamically stable sodium nitrate in the coarse mode, which inhibits the formation of semi-volatile ammonium nitrate in the sub-micron size (fine mode) through competitive consumption of gaseous precursors and change of gas-particle equilibrium (Chen et al., 2016a; Zaveri et al., 2008; Myhre et al., 2006). Compared to the fine particles, coarse particles have a significantly lower extinction efficiency in 60 the visible part of the spectrum (IPCC, 2013; Murphy et al., 1998), the sea-salt-induced ‘re-distribution effect’ thus tends to weaken $\text{DRF}_{\text{nitrate}}$, which counteracts the ‘mass-enhancement effect’. The competition between these two effects will ultimately determine the net impact of sea-salt aerosol on anthropogenic $\text{DRF}_{\text{nitrate}}$. To



the best of our knowledge, this sea-salt-induced ‘re-distribution effect’ is neglected in most global models, due to the computationally expensive calculations of fully dynamic mass transfer between size-resolved
65 particulate nitrate (Adams et al., 2001; Myhre et al., 2006); for more details see Supplementary Information Section S1.

To explore the competition between the sea-salt-induced ‘mass-enhancement effect’ and ‘re-distribution effect’ and the impact of the ‘re-distribution’ process on the nitrate cooling of climate, we conducted a series of sensitivity studies with and without sea-salt aerosol emission for a typical sea-salt event over Europe and
70 North America, using a regional atmospheric chemistry model (WRF-Chem) with a fully dynamic mass transfer approach (Zaveri et al., 2008); see ‘Data & Methods’ for details. A one-year simulation with the EMAC (ECHAM5/MESy Atmospheric Chemistry) model is used to demonstrate the importance of the ‘re-distribution effect’ on a global scale (Jöckel et al., 2010).

75 2. Data & Methods

2.1 Observations

HOPE-Melpitz campaign (HD(CP)² Observational Prototype Experiment, Macke et al., 2017) was carried out during 10-20 September 2013 at Melpitz (12.93°E, 51.53°N, 86 m a.s.l.). Melpitz represents the regional background of central Europe (Spindler et al., 2012), with flat surrounding topography over an area
80 of hundreds of square kilometers, ranging 100-250 m a.s.l.

Size-segregated measurements of particles composition were carried out on 13 September and 18 September, which represent the continental period and marine period, respectively. A five-stage Berner impactor (Hauke, Austria, 0.05-0.14 μm , 0.14-0.42 μm , 0.42-1.2 μm , 1.2-3.5 μm , and 3.5-10 μm ; Berner and Luerzer, 1980) was operated to segregate particles onto ring-like pre-baked (350 °C) aluminium foils
85 with a sampling period of 24 h (00:00-24:00, local time) for detailed chemical analyses (Spindler et al., 2012). The isokinetic inlet for particles with an aerosol dynamic diameter smaller than 10 μm was installed 6 meters above the ground. To compare with modelling results, we use the sum of the particle mass at stage 1-3 (PM_{1,2}, aerosol dynamic diameter smaller than 1.2 μm) to represent fine mode particles and the sum of the mass at stages 4-5 (PM_{1,2-10}, aerosol dynamic diameter smaller between 1.2 and 10 μm) to represent
90 coarse mode particles. The gravimetric mass of the pre-heated aluminium foils was weighted respectively



before and after the sampling process, by a microbalance (UMT-2, Mettler-Toledo, Switzerland). Before each weighting, the aluminium foils were equilibrated for at least 72 hours in a strictly controlled environment with a temperature of 20 ± 1 °C and a relative humidity of $50\pm 5\%$. After an aqueous extraction of foil aliquots, the main water-soluble cations (Na^+ , NH_4^+ , K^+ , Mg^{2+} and Ca^{2+}) were quantified by standard ion chromatography (Neusüß et al., 2000). Likewise, capillary electrophoresis (Neusüß et al., 2000) was carried out to quantify the anions (NO_3^- , SO_4^{2-} and Cl^-). A carbon analyzer (Behr Labor-Technik, Germany) was used to separate and measure the sampled organic and elemental carbon with a two-step thermographic method (modified VDI method 2465 part-2, Spindler et al., 2012). Organic carbon was vaporized at 650 °C for 8 minutes under N_2 and catalytically converted to CO_2 ; the remaining elemental carbon was combusted for another 8 minutes with O_2 at 650 °C. Generated CO_2 was then quantitatively determined using a non-dispersive infrared detector.

2.2 Model description

We performed regional model simulations with the ‘online coupled’ air quality model Weather Research and Forecasting/Chemistry model (WRF-Chem V3.5.1, Grell et al., 2005). WRF-Chem enables more detailed investigation of aerosol-radiation interaction over specific regions at higher horizontal resolution compared with global models, and has been broadly used for investigating aerosol radiative forcing in previous studies (e.g., Archer-Nicholls et al., 2019; Fast et al., 2006; Saide et al., 2012; Gao et al., 2018; Yao et al., 2017; Huang et al., 2015). To investigate the impact of ‘re-distribution effect’ on PMSD and climate effect of nitrate, the fully dynamic aerosol module MOSAIC (Zaveri et al., 2008) was utilized with eight discrete size bins (39-78 nm, 78-156 nm, 156-312 nm, 312-625 nm, 625-1250 nm, 1.25-2.5 μm , 2.5-5 μm , 5-10 μm ; see also Fig. S1), with the online coupled CBMZ (Carbon-Bond Mechanism version Z) gas chemistry scheme (Zaveri and Peters, 1999). The sea-salt emissions computed with the modified Gong scheme (Gong, 2003) were reduced to 10% in the ‘Case_SeasaltOn’, because a previous study (Chen et al., 2016a) has shown that the original Gong scheme overestimates the sea-salt mass concentrations by a factor of ~ 10 over the coastal regions of Europe. The sea-salt emission was turned off in the ‘Case_SeasaltOff’ simulation. We calculate the DRF of anthropogenic nitrate at the top of the atmosphere for both with and without sea-salt presence respectively, based on the difference in the net incoming radiative flux with and without the anthropogenically emitted gas phase precursor NO_x (IPCC, 2013; Xu and Penner, 2012). Only



120 the model results during daytime (07:00-16:00, local time) and under clear-sky condition (cloud optical depth equals to zero) were used for the analyses of DRF in this study.

WRF-Chem calculated aerosol optical depth (AOD) and direct radiative effect of total aerosols based on the internal mixture assumption and taking the hygroscopicity into account. In order to calculate the light extinction coefficient and optical depth for individual aerosol species, we performed the following off-line
125 calculation. The AOD of each species is calculated by integrating light extinction coefficient (σ_{ex}) over all vertical layers. The σ_{ex} of sea-salt (NaCl) and particulate nitrate were calculated with Mie theory, based on their PMSD. Different from the WRF-Chem calculation of total aerosol AOD, external mixture was assumed for nitrate and sea-salt particles when calculating their respective contributions on σ_{ex} or AOD. Hygroscopic growth was also considered, following the κ -Köhler theory (Köhler, 1936; Petters and Kreidenweis, 2007).

130

2.3 European simulation

The European simulations focus on the HOPE-Melpitz campaign period of 10-20 September 2013, during which a sea-salt event that influenced most part of Europe was captured. The simulations are defined by two nested domains with horizontal resolutions of 54 km and 18 km respectively, and 39 vertical layers
135 with model top at 50 hPa. The coarse domain (D01, 30° N – 71.5° N, 30° W – 46° E) covers the North Sea, the European continent and part of North Africa. The inner domain (D02, 38° N – 60° N, 8° W – 28° E, see Fig. 2) covers most of the North Sea and the European continent. The European anthropogenic emission inventories are provided by TNO (www.tno.nl) from the AQMEII project (Air Quality Model Evaluation International Initiative) for PM_{2.5}, PM_{2.5-10}, NO_x, SO₂, CO, NH₃, and non-methane volatile organic
140 compounds (Pouliot et al., 2012; Chen et al., 2018b), and from the EUCAARI project (European Integrated project on Aerosol, Cloud, Climate, and Air Quality Interactions) for particulate organic carbon and elemental carbon (Kulmala et al., 2011). The inventories are with a spatial resolution of 1/8° × 1/16° longitude-latitude. We excluded the point source emissions of elemental carbon in EUCAARI inventory over
145 emissions, meteorological and chemical initial/boundary conditions can be found in the Supplementary Information Section S2. Detailed information about the model configuration is given in Table 1.

In the ‘Case_SeasaltOn’ (with sea-salt emission) of European simulation, modelled [Na⁺] showed good agreement with measurements over coastal region from European Monitoring and Evaluation Programme



(EMEP, <http://www.emep.int>), with a factor (and correlation coefficient) of 0.85 (0.67), 1.16 (0.80) and 0.83 (0.87) respectively for Bilthoven, Kollumerwaard and Vredepeel (Fig. S2). Compared with ground-based measurements at Melpitz and radio-sounding measurements across Europe, the meteorological conditions were well captured by the model (Chen et al., 2016a). Vertical structures of potential temperature and wind speed were realistically reproduced, with correlation coefficients between simulation and measurement results of ~ 0.9 over coastal, German low lands (Melpitz) and northern Poland regions (Chen et al., 2016a). In line with previous studies (Xu and Penner, 2012; Li et al., 2013), the modelled AOD agreed reasonably well with the AERONET observations (AEROSOL ROBOTIC NETWORK, <http://aeronet.gsfc.nasa.gov>). The spatial distribution of AOD can be generally captured by the model ($R=0.64$), although model may overestimate AOD by a geometric mean bias of 70% (see Supplementary Information Section S3 for details).

2.4 North America and global simulations

To investigate the significance of the ‘re-distribution effect’ in a boarder spatial scale, we also conducted WRF-Chem simulation over North America, where high concentration of nitrate was usually observed. We focus on the period of 10-17 January 2015, when strong continental outflow interacted with marine air masses over the Gulf of Mexico. The North American domain covers US, the Gulf of Mexico and part of Pacific and Atlantic oceans, with a horizontal resolution of 36 km. In addition, a one-year simulation with global model (EMAC) was carried out for analysis of the potential impact of ‘re-distribution effect’ on a global scale, although the fully dynamic mass transfer between particle sizes is not considered in EMAC (four size modes rather than eight size bins as applied in the WRF-Chem model). More details of EMAC model and its aerosol module are described in our previous work (Pozzer et al., 2012; Klingmüller et al., 2014; Pringle et al., 2010). The global simulation was run at T106L31 resolution, corresponding to a quadratic Gaussian grid of approximately 1.1 by 1.1 degrees (in latitude and longitude) and with 31 levels in the troposphere. The global emission inventory EDGAR (V4.3, 2010, <http://edgar.jrc.ec.europa.eu>) was used in the North American and global simulations.

3. Results and Discussion

3.1 Sea-salt-induced ‘re-distribution effect’

Marine air masses frequently ($\sim 90\%$) approach Central Europe, and the interaction between



anthropogenic pollutants and sea-salt aerosol commonly happens in the atmosphere (Birmili et al., 2001). In this study, we performed a series of numerical sensitivity experiments during a typical sea-salt transport event from 10 to 20 September 2013 during the HOPE-Melpitz campaign. During the campaign, Central Europe was dominated by continental air masses before 15 September. Subsequently marine air masses started travelling over land on 17 September, and sea-salt aerosol originated from the North Sea and the Baltic Sea was transported to northern Poland and dominated Central Europe on 19 September (Fig. 2). Sea-salt is emitted into the marine planetary boundary layer (PBL) as coarse particles, usually with a short lifetime and a limited transport range. Previous studies showed that the special PBL thermodynamic structure over coastal regions (Ding et al., 2004) can bring sea-salt from the marine PBL to the continental free troposphere, therefore prolonging its lifetime and favoring long-range transport, see the figure 11 of Chen et al. (2016a). Afterwards, the sea-salt aloft could be mixed down to surface layer by the fully developed PBL (Chen et al., 2009; Chen et al., 2016a) and interact with anthropogenic nitrate. Therefore, this transport mechanism broadens the sea-salt-induced ‘re-distribution effect’ on nitrate to a larger spatial scale.

As shown in Fig. 3a and 3b, the ‘Case_SeasaltOn’ simulation successfully reproduces the ‘re-distribution effect’ of nitrate when the dominating air mass changed from a continental to marine type at the Central Europe background site Melpitz. Measurements and model results both show an ~10 times increase of sodium concentration ($[\text{Na}^+]$, indicator of sea-salt aerosol) in the coarse mode when marine air masses approached (Fig. S3). While the nitrate mass fraction in the coarse mode was enhanced by a factor of ~5.5, its concentration ($[\text{NO}_3^-]$) in the fine mode was lowered by ~20% (Fig. 3b). A clear re-distribution of particulate nitrate from fine to coarse mode is found when introducing sea-salt in the ‘Case_SeasaltOn’, with negligible changes in other particulate species except sea-salt (Fig. S1). Conversely, without introducing sea-salt aerosol, the ‘Case_SeasaltOff’ did not capture the ‘re-distribution effect’, and the nitrate mass in the fine mode (~97%) dominated in both continental and marine air masses (Fig. 3c).

3.2 Moderation of nitrate cooling by the ‘re-distribution effect’

Figure 4 shows the strong impact of the ‘re-distribution effect’ on nitrate cooling when marine air mass transported further inland and predominated over Europe on 19 September. Although sea-salt aerosol leads to an overall enhancement of nitrate column loading (~1 mg m⁻², Fig. S4) compared to the ‘Case_SeasaltOff’, the nitrate associated aerosol optical depth ($\text{AOD}_{\text{nitrate}}$) decreases significantly over the relatively polluted



continental regions (Fig. 4a), leading to a strongly weakened cooling effect of nitrate in those regions (positive change in DRF_{nitrate} in Fig. 4b). We find that the regions of reduced AOD_{nitrate} co-locate with the regions of reduced fine mode $[NO_3^-]$ (bluish colored areas in Fig. 4a and 4c). Over a large area of the European continent, the ‘re-distribution effect’ shifts the nitrate PMSD from the fine to the coarse mode (Fig. 4c, 4d), resulting in much less efficient light scattering of nitrate aerosol with a reduced cooling effect. The box with a solid black frame in Fig. 4 marks the northern Poland region, where sea-salt aerosol strongly interacted with anthropogenic precursors of nitrate during the studied sea-salt event. In this region, ‘re-distribution effect’ leads to a decrease of column nitrate loading in the fine mode by $\sim 2.9 \text{ mg m}^{-2}$ (Fig. 4c) accompanied by an increase of $\sim 3.7 \text{ mg m}^{-2}$ in the coarse mode due to the ‘mass-enhancement effect’ (Fig. 4d). Consequently, the anthropogenic AOD_{nitrate} is significantly reduced by up to $\sim 30\%$ with an average reduction of $\sim 22\%$ (~ 0.05 in absolute AOD value, Fig. 4a), despite of a $\sim 0.8 \text{ mg m}^{-2}$ net increase in total nitrate loading. This results in a 5-70% reduction of nitrate cooling, on average by $\sim 26\%$ (Fig. 4b). Our results demonstrate that the sea-salt-induced ‘re-distribution effect’ overwhelms the ‘mass-enhancement effect’ over polluted regions, thus moderating the anthropogenic nitrate cooling.

The resulting decrease of nitrate cooling is non-linear with respect to the sea-salt aerosol loading due to the competition between sea-salt-induced ‘mass-enhancement effect’ and ‘re-distribution effect’. To investigate the net impact of this competition, we performed a series of sensitivity simulations with different sea-salt aerosol emission scaling factors (0, 0.5, 1, 2, 3, 4, 5, 6, 8, and 10, the ones with scaling factors of 0 and 1 being our ‘Case_SeasaltOff’ and ‘Case_SeasaltOn’, respectively). As a surrogate of aerosol DRF, the AOD of nitrate and sea-salt aerosol was calculated offline based on the simulated PMSD (see ‘Data & Methods’). Over the northern Poland region (box with solid frame in Fig. 4), total $[NO_3^-]$ (green dashed line in Fig. 5a) increased continuously as a function of $[Na^+]$, which is in line with previous estimates and clearly shows the ‘mass-enhancement effect’ (Liao and Seinfeld, 2005). However, the ‘re-distribution effect’ overwhelms the ‘mass-enhancement effect’ in this region, and the AOD_{nitrate} drops significantly by $\sim 29\%$ (red solid line in Fig. 5a) when the scaling factor of sea-salt aerosol is 1 (‘Case_SeasaltOn’, being slightly higher than the average $\sim 22\%$ from the on-line calculation, due to the difference in aerosol mixing state, i.e., internal mixing of aerosol compositions in the on-line calculation; and external mixing in the offline calculation). The reduction of AOD_{nitrate} reaches a maximum of $\sim 50\%$ (~ 0.09 in absolute AOD value) when $[Na^+]$ is $\sim 2.5 \mu\text{g m}^{-3}$ or higher, which level of sea-salt aerosol has been often observed in Central Europe



(Fig. 5c, Gustafsson and Franzén, 2000; Neumann et al., 2016; Gantt et al., 2015). A similar net reduction of AOD_{nitrate} is also found for Central Europe (marked in Fig. 2), where the overall moderation is $\sim 13\%$ compared to the ‘Case_SeasaltOff’ (Fig. S5a). To further demonstrate the influence of the ‘re-distribution effect’ on nitrate cooling, we calculate the $\Delta AOD_{\text{nitrate}}$ by re-allocating nitrate mass into different size bins according to the normalized nitrate PMSD simulated in the ‘Case_SeasaltOff’, i.e., by neglecting the ‘re-distribution effect’ ($\Delta AOD_{\text{nitrate}}^*$, pink dashed line in Fig. 5a). A distinct opposite trend, with increasing AOD_{nitrate}^* with $[\text{NO}_3^-]$ (green dashed line), would result by neglecting the ‘re-distribution effect’. For example, instead of a decrease by 29%, the AOD_{nitrate}^* over northern Poland increases by $\sim 8\%$ from the ‘Case_SeasaltOff’ to the ‘Case_SeasaltOn’.

It is also noteworthy that the increase rate of $[\text{NO}_3^-]$ decreases as $[\text{Na}^+]$ further increases and there is even a slight decrease of $[\text{NO}_3^-]$ when $[\text{Na}^+]$ exceeds $\sim 5 \mu\text{g m}^{-3}$ (Fig. 5a). This is mostly due to the consumption of nitrate precursor and stronger deposition of particulate nitrate by ‘re-distribution’ toward larger particles sizes and thus shorter lifetimes. This result is consistent with previous studies showing that lifetime of nitrate radical is significantly reduced in the presence of sea-salt aerosols (Rudich et al., 1998; Ravishankara, 1997). The lifetime of nitrate particles can be shortened from about a week to one day by shifting from the fine to the coarse mode (Croft et al., 2014; Chen et al., 2016b) and hence further moderate nitrate cooling effect. Moreover, coarse mode nitrate associated with highly hygroscopic sea-salt enhances its water uptake (Chen et al., 2018a) and cloud condensation nuclei activation (Xu and Penner, 2012; Wang and Chen, 2019), therefore fasten its deposition and scavenge rate. Itahashi et al. (2016) reported that oxygenated nitrogen deposition can be enhanced by 1.6-2.2 times over ocean regions in East Asia by including sea-salt associated nitrate. Liao and Seinfeld (2005) implied a similar enhancement for sea-salt/dust associated sulfate deposition, which result in a decrease in sulfate concentrations in the downwind regions. Our study implies the enhancement of nitrate deposition. As one can see in Fig. 5a, nitrate concentration (green dashed line) firstly increases with increasing sea-salt and then slightly declines when the amount sea-salt (represented by sodium) exceeds a certain level. An inflection point is observed when sodium concentration approached $5.5 \mu\text{g m}^{-3}$ (sea-salt emission factor = 8), the nitrate starts to decrease as sodium further increases (sea-salt emission factor = 10). The enhancement of nitrate deposition should be the reason of this phenomenon. To demonstrate this, we conducted a sensitivity simulation with aerosol dry deposition turned off. We found that nitrate concentration kept increasing from 10.91 to $11.02 \mu\text{g m}^{-3}$ when



265 sea-salt emission factors increased from 8 to 10, instead of showing a decreasing trend as the simulations
with aerosol dry deposition. This indicates an enhanced deposition of nitrate by interaction with sea-salt
which shortens nitrate lifetime and can further reduce nitrate cooling.

3.3 Competition between ‘re-distribution effect’ and ‘mass-enhancement effect’.

270 As a result of competition between the sea-salt-induced ‘re-distribution effect’ and ‘mass-enhancement
effect’, clear spatial inhomogeneity can be found in Fig. 4. The ‘re-distribution effect’ decreases AOD_{nitrate}
over the polluted continental regions; while the ‘mass-enhancement effect’ increases AOD_{nitrate} mostly over
marine areas (Fig. 4a), although the absolute enhancement is rather small due to the low $[NO_3^-]$ in this
environment. For example, over the Mediterranean Sea (marked by the box with a dashed black frame in
275 Fig. 4), the AOD_{nitrate} increases by ~ 0.01 and the cooling effect of nitrate is amplified by $\sim 0.54 \text{ W m}^{-2}$
(negligible without introducing sea-salt aerosol). Sensitivity study also shows a monotonic increase of
 AOD_{nitrate} with $[Na^+]$ over the Mediterranean Sea (Fig. 5b), indicating a dominant role of the ‘mass-
enhancement effect’ over regions with limited anthropogenic influence.

Thus, abundant sea-salt aerosol and pre-existing fine mode nitrate (as if no sea-salt aerosol influence in
280 the ‘Case_SeasaltOff’) favor an efficient ‘re-distribution effect’ that reduces AOD_{nitrate} and moderates nitrate
cooling. To generalize the net impact of sea-salt-induced ‘re-distribution effect’ and ‘mass-enhancement
effect’ on anthropogenic nitrate cooling, we conducted statistical analysis of the molar ratio between fine
nitrate in the ‘Case_SeasaltOff’ and total sodium in the ‘Case_SeasaltOn’ ($RNS = [NO_3^-]/[Na^+]$ in mol mol^{-1})
with relation to the percentage change of nitrate AOD (surrogate of DRF_{nitrate}) between the two cases, i.e.,
285 $(AOD_{\text{nitrate Case_SeasaltOn}} - AOD_{\text{nitrate Case_SeasaltOff}})/AOD_{\text{nitrate Case_SeasaltOn}}$. We found that the ‘re-distribution
effect’ tends to be strong enough to overwhelm the ‘mass-enhancement effect’ when the RNS value is in the
range of about 1 to 30, corresponding to $\sim 70\%$ of the data points in the European domain, as detailed in
Supplementary Information (Fig. S6a and Section S4). Note that only the surface concentrations were used
for calculating the RNS, because fine mode ammonium nitrate is mostly limited in the surface layer due to
290 emissions of NH_3 are in surface layer. The sea-salt (or sodium) aloft during transport process (as discussed
in section 3.1) did not exert the ‘re-distribution effect’ before being mixed down to surface layer, and should
not be included in the analysis. Therefore, we carried out a statistical analysis with surface nitrate and sodium
concentrations, to draw a more robust conclusion. When the ‘re-distribution effect’ is sufficiently strong, the



net reduction of AOD_{nitrate} may even counteract the AOD enhancement contributed by the additional sea-salt
295 aerosol loading and lead to an overall reduction of total AOD in many regions in Europe (Supplementary
Information Fig. S5b and Section S5).

3.4 The ‘re-distribution effect’ over Europe

Due to the frequent interactions between sea-salt aerosol and polluted air masses (Myhre et al., 2006; Xu
300 and Penner, 2012), the moderation of nitrate cooling is expected to be common over Europe, where the lower
atmosphere is characterized by RNS values between 1 and 30 (Fig. 6). As discussed above (Fig. 5a and Fig.
S5), considerable moderation is expected over inland and Central Europe, where $[Na^+] > 2.5 \mu\text{g m}^{-3}$ is
observed frequently (Gustafsson and Franzén, 2000, also see Fig. 5c). Such moderation could be even more
relevant over coastal and continental outflow regions of North America and South/East Asia (discussed in
305 the next section), where high loadings of nitrate were observed and found to be significantly associated with
sea-salt aerosol (30-90% of total nitrate) (Xu and Penner, 2012).

To quantify the possible overestimation of nitrate radiative forcing when only the sea-salt-induced
‘mass-enhancement effect’ was treated but not the ‘re-distribution effect’, similar statistical analysis (Fig. 6)
is conducted for the percentage change of nitrate AOD between the AOD_{nitrate} in the ‘Case_SeasaltOn’ and
310 the corresponding AOD_{nitrate}^* , i.e. $(AOD_{\text{nitrate}} - AOD_{\text{nitrate}}^*)/AOD_{\text{nitrate}}$. As described before, AOD_{nitrate} stands
for the case where both ‘mass-enhancement’ and ‘re-distribution’ effects have been accounted for the
‘Case_SeasaltOn’, while only the ‘mass-enhancement effect’ is accounted for AOD_{nitrate}^* . Fig. S6b shows
that the AOD_{nitrate}^* could increase by 5-30% when introducing sea-salt and only the ‘mass-enhancement
effect’ is considered. Conversely, the statistics show that the ‘re-distribution effect’ tends to significantly
315 reduce the nitrate AOD by 10-20% when there is abundant sea-salt interacting with anthropogenic nitrate
($RNS < \sim 30$, Fig. 6). Note that this estimation of percentage reduction in AOD_{nitrate} is robust (may be slightly
conservative), despite of the overestimation of particulate nitrate over Europe (Supplementary Information
Section S6). The upper limit of our result is comparable to a previous estimate of 25% reduction of AOD_{nitrate}
by sea-salt aerosol on a global scale by Myhre et al. (2006), where a similar ‘re-distribution effect’ of sea-
320 salt aerosol was evaluated but the simplifications of the mass transfer between fine and coarse modes may
lead to overestimation of the reduction (Supplementary Information Section S1). The ‘re-distribution effect’
becomes rather weak (limited within 10%) as RNS further increased ($RNS > \sim 30$) when marine air masses



are transported further inland.

325 3.5 The ‘re-distribution effect’ over North America and on a global scale

An additional simulation over North America confirms our findings. Similar as over Europe, the sea-salt-induced ‘re-distribution effect’ predominates and reduces AOD_{nitrate} over industrialized and outflow regions of the North America domain (Fig. 7). Generally, similar reduction of AOD_{nitrate} is found over North America due to the sea-salt-induced ‘re-distribution effect’. A monotonous decrease (increase) of column
330 fine (coarse) nitrate loading is observed all over North America and oceanic regions (Fig. 7c and Fig. 7d). This sea-salt-induced ‘re-distribution effect’ overwhelms the ‘mass-enhancement effect’ over most regions and thus reduces AOD_{nitrate} (Fig. 7a) and cooling effect of nitrate especially over the Gulf of Mexico (Fig. 7b), although the total nitrate column loading increases significantly (Fig. S7). This is because the high concentration of nitrate in the continental outflow from North and Central America strongly interacts with
335 sea-salt over the Gulf (Xu and Penner, 2012).

The statistical analysis over North America shows a similar pattern as over Europe (Fig. 8). Meanwhile, different from Europe, there is large fraction of the model results presented in the $RNS > 30$ regime in North America, indicating less regions over North America experience a strong ‘re-distribution effect’. The oceanic influence dominates over western Europe whereas over the North America the more continental air masses
340 (Kottek et al., 2006) may be a possible reason of this. It leads to less interactions of sea-salt with anthropogenic nitrate in North America, and more significant reduction of AOD_{nitrate} over Europe. This result is consistent with a previous study (Myhre et al., 2006). However, there are still chances that sea-salt transport (May et al., 2018) and impact AOD_{nitrate} further inland over North America. On average, only considering the ‘mass-enhancement effect’ but ignoring the ‘re-distribution effect’ may lead to an
345 overestimation of AOD_{nitrate} by more than 20% when $RNS < 1$ and by about 10-20% when $1 < RNS < 30$. This RNS range encompasses most of the coastal and offshore regions of North America and favors ‘re-distribution effect’.

On a global scale, the potential influence of the ‘re-distribution effect’ on DRF_{nitrate} is estimated by a one-year RNS simulation with the EMAC (Klingmüller et al., 2014; Pringle et al., 2010) chemistry-climate
350 model (Fig. 9). In line with the WRF-Chem results, a strong ‘re-distribution effect’ is expected over North America and Europe, especially over the coastal regions with high nitrate loading and RNS values around



1. The coastal and offshore regions of Asia with $1 < \text{RNS} < 30$ may experience strong reductions of $\text{AOD}_{\text{nitrate}}$, where the ‘re-distribution effect’ is expected to overwhelm the ‘mass-enhancement effect’. The influence of sea-salt aerosol becomes negligible over inland Asia where marine air mass influence is small ($\text{RNS} > 30$).

355 For the open sea regions with $\text{RNS} < 0.01$ (white background), nitrate climate effect is not important, due to very limited nitrate loading.

4. Summary and Discussion

The interaction between natural sea-salt aerosols and anthropogenic nitrate leads to the ‘re-distribution effect’, which can shift the particulate nitrate from sub- to super-micron sizes and hence lower its mass light extinction efficiency and shorten its lifetime. This ‘re-distribution effect’ can significantly moderate nitrate cooling.

360

The interaction between natural sea-salt aerosols and anthropogenic nitrate happens frequently over Europe (~90%). We performed a series of sensitivity studies during a typical sea-salt event over Europe, using WRF-Chem model with fully dynamic aerosol mass transfer treatment online-coupled. The ‘re-distribution effect’ of nitrate is observed by field measurements and well captured by the ‘Case_SeasaltOn’ simulation. Over the highly polluted northern Poland region, our sensitivity modelling results show that the ‘re-distribution effect’ can reduce $\text{AOD}_{\text{nitrate}}$ by about 20-30%, or even up to ~50% when the sea-salt event is sufficiently strong. Conversely, if only consider the increase of nitrate mass by introducing sea-salt (‘mass-enhancement effect’) and ignore the ‘re-distribution effect’, nitrate AOD could increase by ~8% or even up to ~30% in a strong sea-salt event. We propose a single parameter, RNS ($[\text{NO}_3^-]/[\text{Na}^+]$ in mol mol^{-1}), to describe the competition between sea-salt-induced ‘re-distribution effect’ and ‘mass-enhancement effect’. In general, (1) the sea-salt-induced ‘mass-enhancement effect’ is dominant over oceanic regions and tends to increase $\text{AOD}_{\text{nitrate}}$ when RNS is lower than 1; (2) the sea-salt-induced ‘re-distribution effect’ on nitrate PMSD can decrease $\text{AOD}_{\text{nitrate}}$ by about 10-20% and overwhelm the ‘mass-enhancement effect’ resulting in a net reduction of $\text{AOD}_{\text{nitrate}}$ when $1 < \text{RNS} < 30$; and (3) the influence of sea-salt aerosol is not significant when RNS is higher than 30. These findings are further confirmed by the sensitivity simulations over North America. The impact of ‘re-distribution effect’ on a global scale is estimated using global simulation of RNS, as shown in Fig. 9. Significant ‘re-distribution effect’ is expected over Europe, the Gulf of Mexico, coastal and offshore regions world-wide, may resulting in reduction of $\text{AOD}_{\text{nitrate}}$ by about 10-20%.

370

375

380



5. Implication

This study highlights the impact of the ‘re-distribution effect’ on moderating nitrate cooling by interacting with natural sea-salt aerosols. A similar ‘re-distribution effect’ may apply to the heterogeneous reaction and consumption of gaseous organic compounds, sulfuric and nitric acids on natural desert dust (Usher et al., 2003;Ponczek and George, 2018;Dupart et al., 2012;Ravishankara, 1997), although non-volatile particulate sulfate does not shift from fine to the coarse mode aerosols. Uptake of acids by dust particles can shorten their lifetimes and reduce their radiative forcing (Liao and Seinfeld, 2005;Harris et al., 2013;Karydis et al., 2016;Abdelkader et al., 2015), which could be significant over inland areas where sea-salt aerosol is lacking. Our results imply the possibility that natural particles (sea-salt aerosol and very likely dust as well) moderate the DRF of anthropogenic aerosols and alter the nitrogen (very likely sulfur also) deposition efficiency (Fig. 1). More comprehensive modelling studies with fully dynamic aerosol mass transfer treatment are needed for improving the assessment of aerosol climate effect accounting for the ‘re-distribution effect’ on a global scale.

395



Acknowledgments

We would like to acknowledge the following funding resources: National Natural Science Foundation
400 of China (91644218), the National Key R&D Program of China (2017YFC0210104) and Guangdong
Innovative and Entrepreneurial Research Team Program (2016ZT06N263). We thank Dr. Konrad Müller
(TROPOS) for his contribution to the aerosol composition measurements. This work was supported by
German Research Ministry (01LK1212C) and the Max Planck Society (MPG). Y. F. C. would also like to
thank the Minerva Program of MPG.

405 Author contributions

Y. F. C. led the study. Y. F. C. and Y. C. conceived and design the study. Y. C. performed the WRF-
Chem model simulations and processed the data. N. M. supported the optical calculation. C. W. supported
the kinetic part of the model simulation and result analyses. A. P. and J. L. provided the EMAC global
simulation. G. S. carried out the aerosol chemical composition observations at Melpitz. Y. C., Y. F. C. and
410 H. S. interpreted the results. All co-authors discussed the results. Y. C. and Y. F. C. wrote the manuscript with
inputs from all co-authors.

Additional information

Correspondence and requests for materials should be addressed to and Y. F. C and Y. C.

Competing financial interests

415 The authors declare no competing financial interests.

Data availability

WRF-Chem model code and FINN fire emissions are openly available for download from the website
www2.acom.ucar.edu. NCEP reanalysis data is openly available for download from the website
https://rda.ucar.edu/. AERONET and aerosol observational datasets are openly available for download from
420 the websites https://aeronet.gsfc.nasa.gov/ and http://ebas.nilu.no/default.aspx. The European emission
inventory is available from AQMEII project (http://aqmeii.jrc.ec.europa.eu/) and EUCAARI project
(https://www.atm.helsinki.fi/eucaari/?q=node/3). The global emission inventory is available from EDGAR
project (http://edgar.jrc.ec.europa.eu). The results of EMAC global model is available from
https://dx.doi.org/10.17635/lancaster/researchdata/297. All data needed to evaluate the conclusions in the
425 paper are present in the paper and/or the Supporting Information. Additional data related to this paper should
be addressed to and Y.F.C and Y.C.



References:

- Abdelkader, M., Metzger, S., Mamouri, R. E., Astitha, M., Barrie, L., Levin, Z., and Lelieveld, J.: Dust–air pollution dynamics over the eastern Mediterranean, *Atmos. Chem. Phys.*, 15, 9173–9189, 10.5194/acp-15-9173-2015, 2015.
- Adams, P. J., Seinfeld, J. H., Koch, D., Mickley, L., and Jacob, D.: General circulation model assessment of direct radiative forcing by the sulfate-nitrate-ammonium-water inorganic aerosol system, *Journal of Geophysical Research: Atmospheres*, 106, 1097–1111, 10.1029/2000JD900512, 2001.
- Archer-Nicholls, S., Lowe, D., Lacey, F., Kumar, R., Xiao, Q., Liu, Y., Carter, E., Baumgartner, J., and Wiedinmyer, C.: Radiative Effects of Residential Sector Emissions in China: Sensitivity to Uncertainty in Black Carbon Emissions, *Journal of Geophysical Research: Atmospheres*, 124, 5029–5044, 10.1029/2018JD030120, 2019.
- Bauer, S. E., Koch, D., Unger, N., Metzger, S. M., Shindell, D. T., and Streets, D. G.: Nitrate aerosols today and in 2030: a global simulation including aerosols and tropospheric ozone, *Atmos. Chem. Phys.*, 7, 5043–5059, 10.5194/acp-7-5043-2007, 2007.
- Bellouin, N., Rae, J., Jones, A., Johnson, C., Haywood, J., and Boucher, O.: Aerosol forcing in the Climate Model Intercomparison Project (CMIP5) simulations by HadGEM2-ES and the role of ammonium nitrate, *Journal of Geophysical Research: Atmospheres*, 116, D20206, 10.1029/2011JD016074, 2011.
- Berner, A., and Luerzer, C.: Mass size distributions of traffic aerosols at Vienna, *The Journal of Physical Chemistry*, 84, 2079–2083, 10.1021/j100453a016, 1980.
- Birmili, W., Wiedensohler, A., Heintzenberg, J., and Lehmann, K.: Atmospheric particle number size distribution in central Europe: Statistical relations to air masses and meteorology, *Journal of Geophysical Research*, 106, 32005–32018, DOI: 10.1029/2000JD000220, 2001.
- Chen, Y., Zhao, C., Zhang, Q., Deng, Z. Z., Huang, M. Y., and Ma, X. C.: Aircraft study of mountain chimney effect of Beijing, china, *Journal of Geophysical Research: Atmospheres*, 114, 10.1029/2008JD010610, 2009.
- Chen, Y., Cheng, Y., Ma, N., Wolke, R., Nordmann, S., Schüttauf, S., Ran, L., Wehner, B., Birmili, W., van der Gon, H. A. C. D., Mu, Q., Barthel, S., Spindler, G., Stieger, B., Müller, K., Zheng, G. J., Pöschl, U., Su, H., and Wiedensohler, A.: Sea salt emission, transport and influence on size-segregated nitrate simulation: a case study in northwestern Europe by WRF-Chem, *Atmos. Chem. Phys.*, 16, 12081–12097, 10.5194/acp-16-12081-2016, 2016a.
- Chen, Y., Cheng, Y. F., Nordmann, S., Birmili, W., Denier van der Gon, H. A. C., Ma, N., Wolke, R., Wehner, B., Sun, J., Spindler, G., Mu, Q., Pöschl, U., Su, H., and Wiedensohler, A.: Evaluation of the size segregation of elemental carbon (EC) emission in Europe: influence on the simulation of EC long-range transportation, *Atmos. Chem. Phys.*, 16, 1823–1835, 10.5194/acp-16-1823-2016, 2016b.
- Chen, Y., Wild, O., Wang, Y., Ran, L., Teich, M., Größ, J., Wang, L., Spindler, G., Herrmann, H., van Pinxteren, D., McFiggans, G., and Wiedensohler, A.: The influence of impactor size cut-off shift caused by hygroscopic growth on particulate matter loading and composition measurements, *Atmospheric Environment*, 195, 141–148, <https://doi.org/10.1016/j.atmosenv.2018.09.049>, 2018a.
- Chen, Y., Wolke, R., Ran, L., Birmili, W., Spindler, G., Schröder, W., Su, H., Cheng, Y., Tegen, I., and Wiedensohler, A.: A parameterization of the heterogeneous hydrolysis of N₂O₅ for mass-based aerosol models: improvement of particulate nitrate prediction, *Atmos. Chem. Phys.*, 18, 673–689, 10.5194/acp-18-673-2018, 2018b.
- Chou, M.-D., Suarez, M. J., Ho, C.-H., Yan, M. M. H., and Lee, K.-T.: Parameterizations for Cloud Overlapping and Shortwave Single-Scattering Properties for Use in General Circulation and Cloud Ensemble Models, *Journal of Climate*, 11, 202–214, 10.1175/1520-0442(1998)011<0202:PFCOAS>2.0.CO;2, 1998.
- Croft, B., Pierce, J. R., and Martin, R. V.: Interpreting aerosol lifetimes using the GEOS-Chem model and constraints from radionuclide measurements, *Atmospheric Chemistry and Physics*, 14, 4313–4325, 2014.
- Ding, A., Wang, T., Zhao, M., Wang, T., and Li, Z.: Simulation of sea-land breezes and a discussion of their implications on the transport of air pollution during a multi-day ozone episode in the Pearl River Delta of China, *Atmospheric Environment*, 38, 6737–6750,



- <https://doi.org/10.1016/j.atmosenv.2004.09.017>, 2004.
- Dupart, Y., King, S. M., Nekat, B., Nowak, A., Wiedensohler, A., Herrmann, H., David, G., Thomas, B., Miffre, A., Rairoux, P., D'Anna, B., and George, C.: Mineral dust photochemistry induces nucleation events in the presence of SO₂, Proceedings of the National Academy of Sciences, 109, 20842-20847, 10.1073/pnas.1212297109, 2012.
- Fast, J. D., Gustafson Jr, W. I., Easter, R. C., Zaveri, R. A., Barnard, J. C., Chapman, E. G., Grell, G. A., and Peckham, S. E.: Evolution of ozone, particulates, and aerosol direct radiative forcing in the vicinity of Houston using a fully coupled meteorology-chemistry-aerosol model, Journal of Geophysical Research: Atmospheres, 111, 10.1029/2005JD006721, 2006.
- Forster, P., Ramaswamy, V., Artaxo, P., Bernsten, T., Betts, R., Fahey, D. W., Haywood, J., Lean, J., Lowe, D. C., Myhre, G., Nganga, J., Prinn, R., Raga, G., Schulz, M., and Van Dorland, R.: Changes in Atmospheric Constituents and in Radiative Forcing, in: Climate Change 2007: The Physical Science Basis. Contribution of Working Group I to the Fourth Assessment Report of the Intergovernmental Panel on Climate Change, edited by: Solomon, S., Qin, D., Manning, M., Chen, Z., Marquis, M., Averyt, K. B., Tignor, M., and Miller, H. L., Cambridge University Press, Cambridge, United Kingdom and New York, NY, USA, 2007.
- Gantt, B., Kelly, J. T., and Bash, J. O.: Updating sea spray aerosol emissions in the Community Multiscale Air Quality (CMAQ) model version 5.0.2, Geosci. Model Dev., 8, 3733-3746, 10.5194/gmd-8-3733-2015, 2015.
- Gao, M., Ji, D., Liang, F., and Liu, Y.: Attribution of aerosol direct radiative forcing in China and India to emitting sectors, Atmospheric Environment, 190, 35-42, <https://doi.org/10.1016/j.atmosenv.2018.07.011>, 2018.
- Gong, S. L.: A parameterization of sea-salt aerosol source function for sub- and super-micron particles, Global Biogeochemical Cycles, 17, 10.1029/2003GB002079, 2003.
- Grell, G. A., Peckham, S. E., Schmitz, R., McKeen, S. A., Frost, G., Skamarock, W. C., and Eder, B.: Fully coupled “online” chemistry within the WRF model, Atmospheric Environment, 39, 6957-6975, <http://dx.doi.org/10.1016/j.atmosenv.2005.04.027>, 2005.
- Gustafsson, M. E. R., and Franzén, L. G.: Inland transport of marine aerosols in southern Sweden, Atmospheric Environment, 34, 313-325, [http://dx.doi.org/10.1016/S1352-2310\(99\)00198-3](http://dx.doi.org/10.1016/S1352-2310(99)00198-3), 2000.
- Harris, E., Sinha, B., van Pinxteren, D., Tilgner, A., Fomba, K. W., Schneider, J., Roth, A., Gnauk, T., Fahlbusch, B., Mertes, S., Lee, T., Collett, J., Foley, S., Borrmann, S., Hoppe, P., and Herrmann, H.: Enhanced Role of Transition Metal Ion Catalysis During In-Cloud Oxidation of SO₂, Science, 340, 727-730, 10.1126/science.1230911, 2013.
- Hauglustaine, D. A., Balkanski, Y., and Schulz, M.: A global model simulation of present and future nitrate aerosols and their direct radiative forcing of climate, Atmos. Chem. Phys., 14, 11031-11063, 10.5194/acp-14-11031-2014, 2014.
- Haywood, J., and Schulz, M.: Causes of the reduction in uncertainty in the anthropogenic radiative forcing of climate between IPCC (2001) and IPCC (2007), Geophysical Research Letters, 34, L20701, 10.1029/2007GL030749, 2007.
- Hong, S.-Y., Noh, Y., and Dudhia, J.: A new vertical diffusion package with an explicit treatment of entrainment processes, Mon. Weather Rev., 134, 2318-2341, 2006.
- Huang, X., Song, Y., Zhao, C., Cai, X., Zhang, H., and Zhu, T.: Direct Radiative Effect by Multicomponent Aerosol over China, Journal of Climate, 28, 3472-3495, 10.1175/JCLI-D-14-00365.1, 2015.
- IPCC: Climate Change 2013: The Physical Science Basis. Contribution of Working Group I to the Fifth Assessment Report of the Intergovernmental Panel on Climate Change, Report, edited by: Stocker, T. F., Qin, D. H., Plattner, G. K., Tignor, M. M. B., Allen, S. K., Boschung, J., Nauels, A., Xia, Y., Bex, V., and Midgley, P. M., Cambridge University Press, New York, available at: <http://www.ipcc.ch/report/ar5> (last access: 10 September, 2016), 2013.
- Itahashi, S., Hayami, H., Uno, I., Pan, X., and Uematsu, M.: Importance of coarse-mode nitrate produced via sea salt as atmospheric input to East Asian oceans, Geophysical Research Letters, 10.1002/2016GL068722, 2016.
- Jacobson, M. Z.: Global direct radiative forcing due to multicomponent anthropogenic and natural aerosols, Journal of Geophysical Research: Atmospheres, 106, 1551-1568, 10.1029/2000JD900514, 2001.



- Jöckel, P., Kerkweg, A., Pozzer, A., Sander, R., Tost, H., Riede, H., Baumgaertner, A., Gromov, S., and Kern, B.: Development cycle 2 of the Modular Earth Submodel System (MESSy2), *Geosci. Model Dev.*, 3, 717-752, 10.5194/gmd-3-717-2010, 2010.
- Karydis, V. A., Tsimpidi, A. P., Pozzer, A., Astitha, M., and Lelieveld, J.: Effects of mineral dust on global atmospheric nitrate concentrations, *Atmos. Chem. Phys.*, 16, 1491-1509, 10.5194/acp-16-1491-2016, 2016.
- Klingmüller, K., Steil, B., Brühl, C., Tost, H., and Lelieveld, J.: Sensitivity of aerosol radiative effects to different mixing assumptions in the AEROPT 1.0 submodel of the EMAC atmospheric-chemistry–climate model, *Geosci. Model Dev.*, 7, 2503-2516, 10.5194/gmd-7-2503-2014, 2014.
- Köhler, H.: The nucleus in and the growth of hygroscopic droplets, *Transactions of the Faraday Society*, 32, 1152-1161, 10.1039/TF9363201152, 1936.
- Kok, J. F., Ridley, D. A., Zhou, Q., Miller, R. L., Zhao, C., Heald, C. L., Ward, D. S., Albani, S., and Haustein, K.: Smaller desert dust cooling effect estimated from analysis of dust size and abundance, *Nature Geosci.*, 10, 274-278, 10.1038/ngeo2912, 2017.
- Kottke, M., Grieser, J., Beck, C., Rudolf, B., and Rubel, F.: World Map of the Köppen-Geiger climate classification updated, *Meteorologische Zeitschrift*, 15, 259-263, 10.1127/0941-2948/2006/0130, 2006.
- Kulmala, M., Asmi, A., Lappalainen, H. K., Baltensperger, U., Brenguier, J. L., Facchini, M. C., Hansson, H. C., Hov, Ø., O'Dowd, C. D., Pöschl, U., Wiedensohler, A., Boers, R., Boucher, O., de Leeuw, G., Denier van der Gon, H. A. C., Feichter, J., Krejci, R., Laj, P., Lihavainen, H., Lohmann, U., McFiggans, G., Mentel, T., Pilinis, C., Riipinen, I., Schulz, M., Stohl, A., Swietlicki, E., Vignati, E., Alves, C., Amann, M., Ammann, M., Arabas, S., Artaxo, P., Baars, H., Beddows, D. C. S., Bergström, R., Beukes, J. P., Bilde, M., Burkhardt, J. F., Canonaco, F., Clegg, S. L., Coe, H., Crumeyrolle, S., D'Anna, B., Decesari, S., Gilardoni, S., Fischer, M., Fjaeraa, A. M., Fountoukis, C., George, C., Gomes, L., Halloran, P., Hamburger, T., Harrison, R. M., Herrmann, H., Hoffmann, T., Hoose, C., Hu, M., Hyvärinen, A., Hörrak, U., Iinuma, Y., Iversen, T., Josipovic, M., Kanakidou, M., Kiendler-Scharr, A., Kirkevåg, A., Kiss, G., Klimont, Z., Kolmonen, P., Komppula, M., Kristjánsson, J. E., Laakso, L., Laaksonen, A., Labonnote, L., Lanz, V. A., Lehtinen, K. E. J., Rizzo, L. V., Makkonen, R., Manninen, H. E., McMeeking, G., Merikanto, J., Minikin, A., Mirme, S., Morgan, W. T., Nemitz, E., O'Donnell, D., Panwar, T. S., Pawlowska, H., Petzold, A., Pienaar, J. J., Pio, C., Plass-Duelmer, C., Prévôt, A. S. H., Pryor, S., Reddington, C. L., Roberts, G., Rosenfeld, D., Schwarz, J., Seland, Ø., Sellegri, K., Shen, X. J., Shiraiwa, M., Siebert, H., Sierau, B., Simpson, D., Sun, J. Y., Topping, D., Tunved, P., Vaattovaara, P., Vakkari, V., Veefkind, J. P., Visschedijk, A., Vuollekoski, H., Vuolo, R., Wehner, B., Wildt, J., Woodward, S., Worsnop, D. R., van Zadelhoff, G. J., Zardini, A. A., Zhang, K., van Zyl, P. G., Kerminen, V. M., S Carslaw, K., and Pandis, S. N.: General overview: European Integrated project on Aerosol Cloud Climate and Air Quality interactions (EUCAARI) – integrating aerosol research from nano to global scales, *Atmos. Chem. Phys.*, 11, 13061-13143, 10.5194/acp-11-13061-2011, 2011.
- Li, S., Garay, M. J., Chen, L., Rees, E., and Liu, Y.: Comparison of GEOS-Chem aerosol optical depth with AERONET and MISR data over the contiguous United States, *Journal of Geophysical Research: Atmospheres*, 118, 2112-2128, 10.1029/2012JD018208, 2013.
- Liao, H., Seinfeld, J. H., Adams, P. J., and Mickley, L. J.: Global radiative forcing of coupled tropospheric ozone and aerosols in a unified general circulation model, *Journal of Geophysical Research: Atmospheres*, 109, D16207, 10.1029/2003JD004456, 2004.
- Liao, H., and Seinfeld, J. H.: Global impacts of gas-phase chemistry-aerosol interactions on direct radiative forcing by anthropogenic aerosols and ozone, *Journal of Geophysical Research: Atmospheres*, 110, D18208, 10.1029/2005JD005907, 2005.
- Lin, Y., Farley, R., and Orville, H.: Bulk Parameterization of the Snow Field in a Cloud Model, *J. Clim. Appl. Meteorol.*, 22, 1065-1092, 1983.
- Lowe, D., Archer-Nicholls, S., Morgan, W., Allan, J., Utembe, S., Ouyang, B., Aruffo, E., Le Breton, M., Zaveri, R. A., Di Carlo, P., Percival, C., Coe, H., Jones, R., and McFiggans, G.: WRF-Chem model predictions of the regional impacts of N₂O₅ heterogeneous processes on night-time chemistry over north-western Europe, *Atmos. Chem. Phys.*, 15, 1385-1409, 10.5194/acp-15-1385-2015, 2015.
- Macke, A., Seifert, P., Baars, H., Barthlott, C., Beekmans, C., Behrendt, A., Bohn, B., Brueck, M., Bühl, J.,



- Crewell, S., Damian, T., Deneke, H., Düsing, S., Foth, A., Di Girolamo, P., Hammann, E., Heinze, R., Hirsikko, A., Kalisch, J., Kalthoff, N., Kinne, S., Kohler, M., Löhnert, U., Madhavan, B. L., Maurer, V., Muppa, S. K., Schween, J., Serikov, I., Siebert, H., Simmer, C., Späth, F., Steinke, S., Trümner, K., Trömel, S., Wehner, B., Wieser, A., Wulfmeyer, V., and Xie, X.: The HD(CP)2 Observational Prototype Experiment (HOPE) – an overview, *Atmos. Chem. Phys.*, 17, 4887-4914, 10.5194/acp-17-4887-2017, 2017.
- May, N. W., Gansch, M. J., Olson, N., Bondy, A. L., Kirpes, R. M., Bertman, S., China, S., Laskin, A., Hopke, P. K., Ault, A. P., and Pratt, K. A.: Unexpected contributions of sea spray and lake spray aerosol to inland particulate matter, *Environmental Science & Technology Letters*, 10.1021/acs.estlett.8b00254, 2018.
- Murphy, D. M., Anderson, J. R., Quinn, P. K., McInnes, L. M., Brechtel, F. J., Kreidenweis, S. M., Middlebrook, A. M., Posfai, M., Thomson, D. S., and Buseck, P. R.: Influence of sea-salt on aerosol radiative properties in the Southern Ocean marine boundary layer, *Nature*, 392, 62-65, 1998.
- Myhre, G., Grini, A., and Metzger, S.: Modelling of nitrate and ammonium-containing aerosols in presence of sea salt, *Atmos. Chem. Phys.*, 6, 4809-4821, 10.5194/acp-6-4809-2006, 2006.
- Myhre, G., Samset, B. H., Schulz, M., Balkanski, Y., Bauer, S., Bernsten, T. K., Bian, H., Bellouin, N., Chin, M., Diehl, T., Easter, R. C., Feichter, J., Ghan, S. J., Hauglustaine, D., Iversen, T., Kinne, S., Kirkevåg, A., Lamarque, J. F., Lin, G., Liu, X., Lund, M. T., Luo, G., Ma, X., van Noije, T., Penner, J. E., Rasch, P. J., Ruiz, A., Seland, Ø., Skeie, R. B., Stier, P., Takemura, T., Tsigaridis, K., Wang, P., Wang, Z., Xu, L., Yu, H., Yu, F., Yoon, J. H., Zhang, K., Zhang, H., and Zhou, C.: Radiative forcing of the direct aerosol effect from AeroCom Phase II simulations, *Atmos. Chem. Phys.*, 13, 1853-1877, 10.5194/acp-13-1853-2013, 2013.
- Neumann, D., Matthias, V., Bieser, J., Aulinger, A., and Quante, M.: A comparison of sea salt emission parameterizations in northwestern Europe using a chemistry transport model setup, *Atmos. Chem. Phys.*, 16, 9905-9933, 10.5194/acp-16-9905-2016, 2016.
- Neusüß, C., Weise, D., Birmili, W., Wex, H., Wiedensohler, A., and Covert, D. S.: Size-segregated chemical, gravimetric and number distribution-derived mass closure of the aerosol in Sagres, Portugal during ACE-2, *Tellus B*, 52, 169-184, 10.1034/j.1600-0889.2000.00039.x, 2000.
- O'Dowd, C. D., Smith, M. H., Consterdine, I. E., and Lowe, J. A.: Marine aerosol, sea-salt, and the marine sulphur cycle: a short review, *Atmospheric Environment*, 31, 73-80, [http://dx.doi.org/10.1016/S1352-2310\(96\)00106-9](http://dx.doi.org/10.1016/S1352-2310(96)00106-9), 1997.
- Petters, M. D., and Kreidenweis, S. M.: A single parameter representation of hygroscopic growth and cloud condensation nucleus activity, *Atmos. Chem. Phys.*, 7, 1961-1971, 10.5194/acp-7-1961-2007, 2007.
- Ponczek, M., and George, C.: Kinetics and Product Formation during the Photooxidation of Butanol on Atmospheric Mineral Dust, *Environmental Science & Technology*, 52, 5191-5198, 10.1021/acs.est.7b06306, 2018.
- Pouliot, G., Pierce, T., Denier van der Gon, H., Schaap, M., Moran, M., and Nopmongkol, U.: Comparing emission inventories and model-ready emission datasets between Europe and North America for the AQMEII project, *Atmospheric Environment*, 53, 4-14, <http://dx.doi.org/10.1016/j.atmosenv.2011.12.041>, 2012.
- Pozzer, A., de Meij, A., Pringle, K. J., Tost, H., Doering, U. M., van Aardenne, J., and Lelieveld, J.: Distributions and regional budgets of aerosols and their precursors simulated with the EMAC chemistry-climate model, *Atmos. Chem. Phys.*, 12, 961-987, 10.5194/acp-12-961-2012, 2012.
- Pringle, K. J., Tost, H., Message, S., Steil, B., Giannadaki, D., Nenes, A., Fountoukis, C., Stier, P., Vignati, E., and Lelieveld, J.: Description and evaluation of GMXc: a new aerosol submodel for global simulations (v1), *Geosci. Model Dev.*, 3, 391-412, 10.5194/gmd-3-391-2010, 2010.
- Ravishankara, A. R.: Heterogeneous and Multiphase Chemistry in the Troposphere, *Science*, 276, 1058-1065, 10.1126/science.276.5315.1058, 1997.
- Rudich, Y., Talukdar, R. K., and Ravishankara, A. R.: Multiphase chemistry of NO₃ in the remote troposphere, *Journal of Geophysical Research: Atmospheres*, 103, 16133-16143, 10.1029/98JD01280, 1998.
- Saide, P. E., Spak, S. N., Carmichael, G. R., Mena-Carrasco, M. A., Yang, Q., Howell, S., Leon, D. C., Snider, J. R., Bandy, A. R., Collett, J. L., Benedict, K. B., de Szoeke, S. P., Hawkins, L. N., Allen, G., Crawford, I., Crosier, J., and Springston, S. R.: Evaluating WRF-Chem aerosol indirect effects



- in Southeast Pacific marine stratocumulus during VOCALS-REx, *Atmos. Chem. Phys.*, 12, 3045-3064, 10.5194/acp-12-3045-2012, 2012.
- Seinfeld, J. H., and Pandis, S. N.: *Atmospheric Chemistry and Physics: From Air Pollution to Climate Change*, John Wiley & Sons, New York, 2nd Edn., 2006.
- Spindler, G., Gnauk, T., Grüner, A., Iinuma, Y., Müller, K., Scheinhardt, S., and Herrmann, H.: Size-segregated characterization of PM10 at the EMEP site Melpitz (Germany) using a five-stage impactor: a six year study, *J Atmos Chem*, 69, 127-157, 10.1007/s10874-012-9233-6, 2012.
- Streets, D. G., Shindell, D. T., Lu, Z., and Faluvegi, G.: Radiative forcing due to major aerosol emitting sectors in China and India, *Geophysical Research Letters*, 40, 4409-4414, 10.1002/grl.50805, 2013.
- Usher, C. R., Michel, A. E., and Grassian, V. H.: Reactions on Mineral Dust, *Chemical Reviews*, 103, 4883-4940, 10.1021/cr020657y, 2003.
- van Dorland, R., Dentener, F. J., and Lelieveld, J.: Radiative forcing due to tropospheric ozone and sulfate aerosols, *Journal of Geophysical Research: Atmospheres*, 102, 28079-28100, 10.1029/97JD02499, 1997.
- Wang, Y., and Chen, Y.: Significant Climate Impact of Highly Hygroscopic Atmospheric Aerosols in Delhi, India, *Geophysical Research Letters*, 0, 10.1029/2019GL082339, 2019.
- Wild, O., Zhu, X., and Prather, M. J.: Fast-J: Accurate Simulation of In- and Below-Cloud Photolysis in Tropospheric Chemical Models, *J. Atmos. Chem.*, 37, 245-282, 2000.
- Xu, L., and Penner, J. E.: Global simulations of nitrate and ammonium aerosols and their radiative effects, *Atmos. Chem. Phys.*, 12, 9479-9504, 10.5194/acp-12-9479-2012, 2012.
- Yao, H., Song, Y., Liu, M., Archer-Nicholls, S., Lowe, D., McFiggans, G., Xu, T., Du, P., Li, J., Wu, Y., Hu, M., Zhao, C., and Zhu, T.: Direct radiative effect of carbonaceous aerosols from crop residue burning during the summer harvest season in East China, *Atmos. Chem. Phys.*, 17, 5205-5219, 10.5194/acp-17-5205-2017, 2017.
- Zaveri, R. A., and Peters, L. K.: A new lumped structure photochemical mechanism for large-scale applications, *J. Geophys. Res.*, 104, 30387-30415, 1999.
- Zaveri, R. A., Easter, R. C., Fast, J. D., and Peters, L. K.: Model for Simulating Aerosol Interactions and Chemistry (MOSAIC), *Journal of Geophysical Research: Atmospheres*, 113, 10.1029/2007JD008782, 2008.



Table 1. Configurations of WRF-Chem

Physics	WRF options
Micro physics	Lin scheme (Lin, 1983)
Boundary layer	YSU (Hong, 2006)
Surface	Rapid Update Cycle (RUC) land surface model
Shortwave radiation	Goddard shortwave (Chou et al., 1998)
Longwave radiation	New Goddard scheme
Cumulus	Grell 3D
Urban	3-category UCM

Chemistry and Aerosol	Chem options
Aerosol module	MOSAIC with 8 bins (Zaveri et al., 2008)
Gas-phase mechanism	CBMZ (Zaveri and Peters, 1999)
Photolytic rate	Fast-J photolysis scheme (Wild et al., 2000)
Sea salt emission	Gong scheme (Gong, 2003)

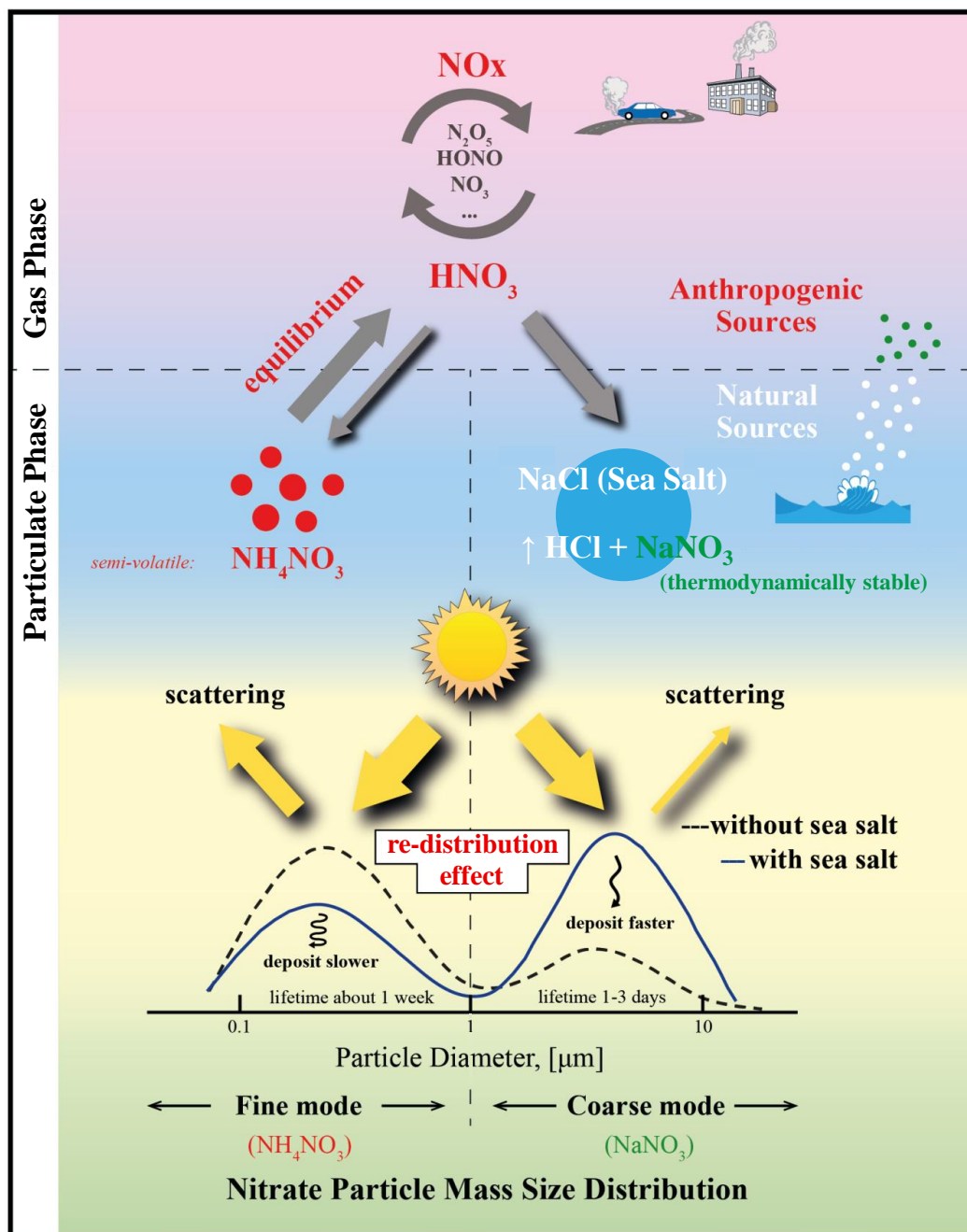


Fig. 1. Concept of the sea-salt aerosol induced 're-distribution effect'.

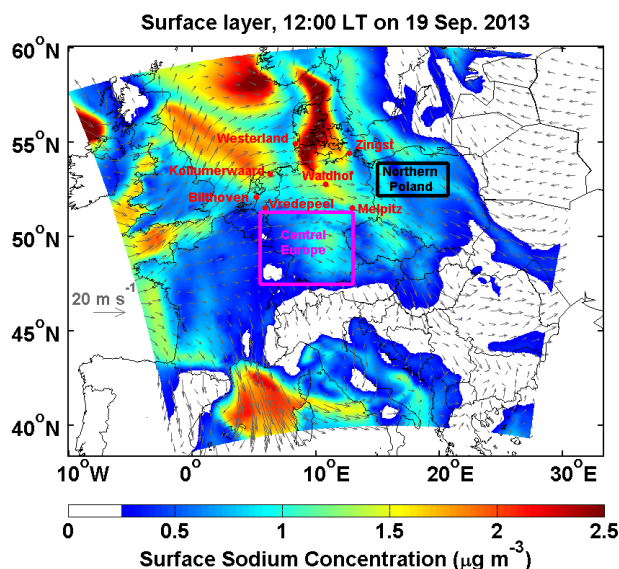


Fig. 2. Surface sodium mass concentration over Europe domain at 12:00 local time (LT) on 19 September 2013. The 10-meter wind is indicated by the grey arrows. The results are based on the ‘Case_SeasaltOn’. Westerland, Waldhof, Zingst, Bithoven, Kollumerwaard, Vredepeel, Melpitz, Central Europe and the northern Poland regions are marked.

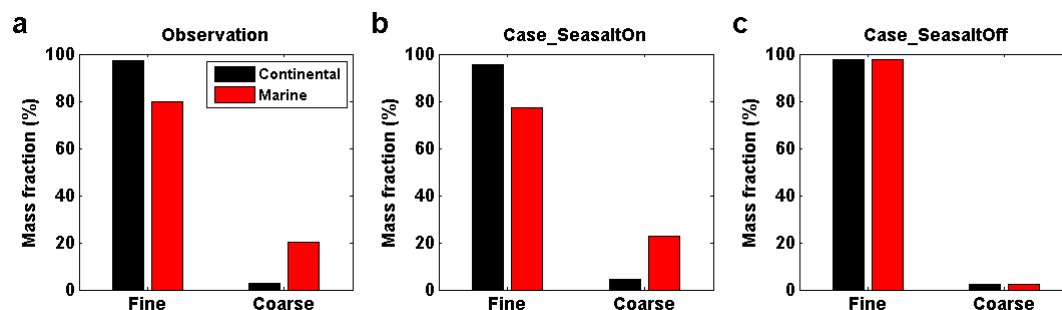


Fig. 3. Observed and simulated mass fraction of particulate nitrate in fine and coarse modes at Melpitz, Germany. **a.** Observation based on the Berner impactor measurements. **b.** WRF-Chem ‘Case_SeasaltOn’ simulation, i.e., with sea-salt emission. **c.** WRF-Chem ‘Case_SeasaltOff’ simulation, i.e., without sea-salt emission. The results are grouped into continental (black bar) and marine (red bar) air mass types, respectively. According to the size-cuts of the Berner impactor, the size ranges of the fine and coarse mode particles are defined as $PM_{1.2}$ (particles with an aerodynamic diameter smaller than $1.2 \mu m$) and $PM_{1.2-10}$ (particles with an aerodynamic diameter larger than $1.2 \mu m$ and smaller than $10 \mu m$), respectively.

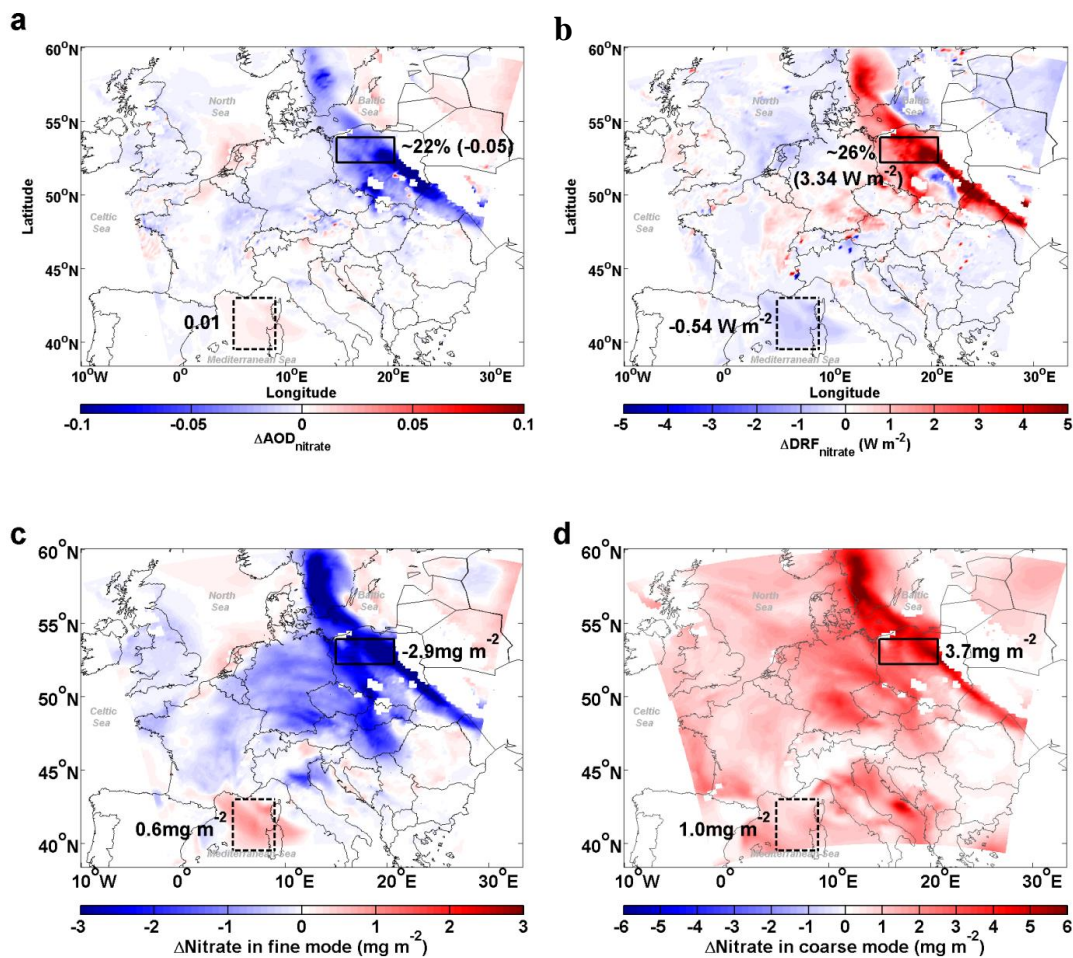


Fig. 4. Influence of sea-salt on the abundance and direct radiative forcing of nitrate. Differences (‘Case_SeasaltOn’ – ‘Case_SeasaltOff’) between simulations with and without sea-salt emission in aerosol optical depth ($\Delta AOD_{\text{nitrate}}$, **a**), direct radiative forcing ($\Delta DRF_{\text{nitrate}}$, **b**), and column loading of nitrate ($\Delta \text{Nitrate}$) for the fine (**c**) and coarse (**d**) mode particles, during daytime, i.e., 07:00-16:00 local time (LT) on 19 September 2013. The northern Poland and Mediterranean regions are marked by boxes with solid and dashed black frames, respectively.

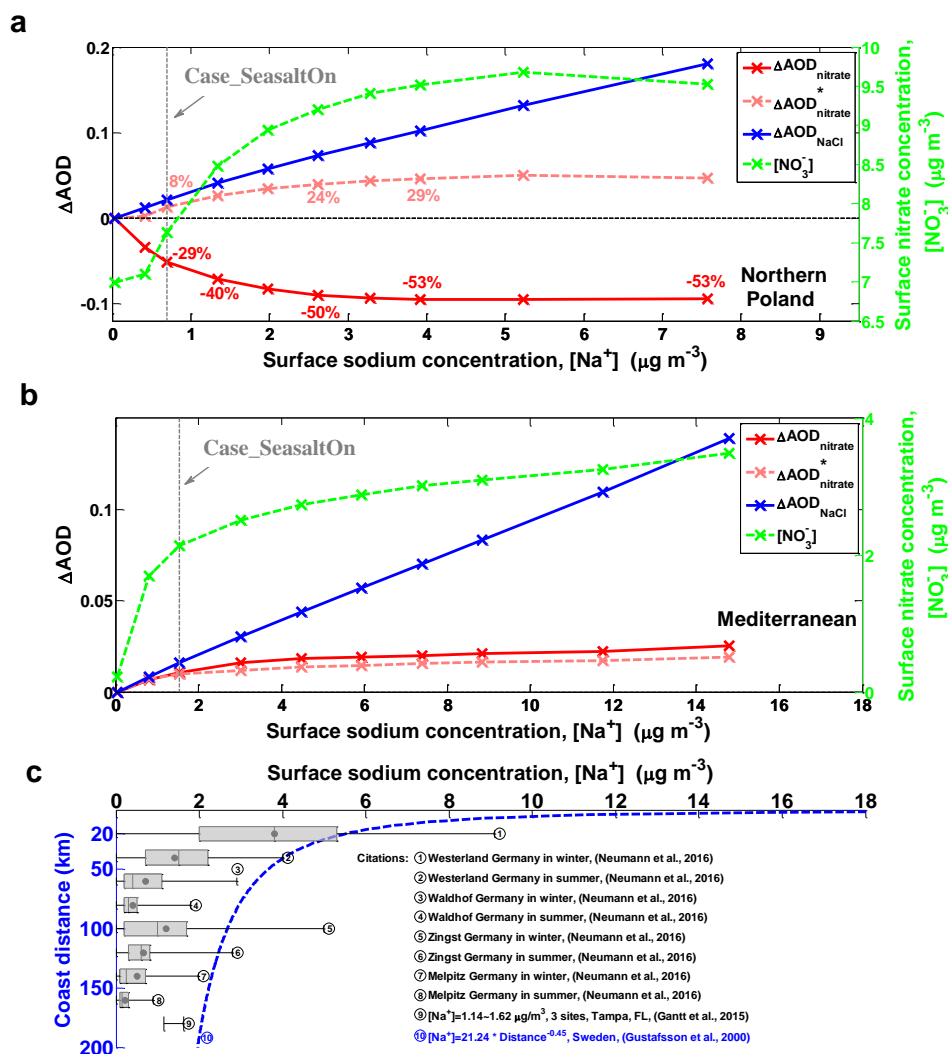


Fig. 5. Sensitivity of aerosol optical depth (ΔAOD) as a function of sodium mass concentration ($[Na^+]$). Differences between the ‘Case_SeasaltOff’ and sensitivity cases (sea-salt emission with different scaling factors) for different aerosol components, i.e., nitrate ($\Delta AOD_{nitrate}$) and sea-salt (ΔAOD_{NaCl}): ΔAOD (sensitivity case – ‘Case_SeasaltOff’) versus $[Na^+]$ over northern Poland (**a**) and Mediterranean regions (**b**), respectively. The model results shown here are averages over a sea-salt event during daytime (07:00-16:00 LT) on 19 September 2013. The results of surface $[NO_3^-]$ are indicated by the green dashed line. Here, the ‘Case_SeasaltOff’ is the reference case and the ‘Case_SeasaltOn’ is marked. Note: $\Delta AOD_{nitrate}^*$ (pink dashed line) indicates the ΔAOD of nitrate calculated by re-allocating nitrate mass into different size bins according to the normalized nitrate particle mass size distribution simulated in ‘Case_SeasaltOff’ (i.e., without ‘re-distribution effect’). **c**, The measured $[Na^+]$ at different sites over Sweden as a function of coast distance, and in Germany (marked in Fig. 2) and US. The box-whisker plots of the references ①-⑧ indicate the median, mean (black dot), 25% percentile, 75% percentile, maximum and minimum. The error bar of the reference ⑨ indicates the range. The blue dashed line of the reference ⑩ indicates the statistically empirical function of $[Na^+]$ with the distance from coast, based on the network measurements of 16 sites in Sweden.

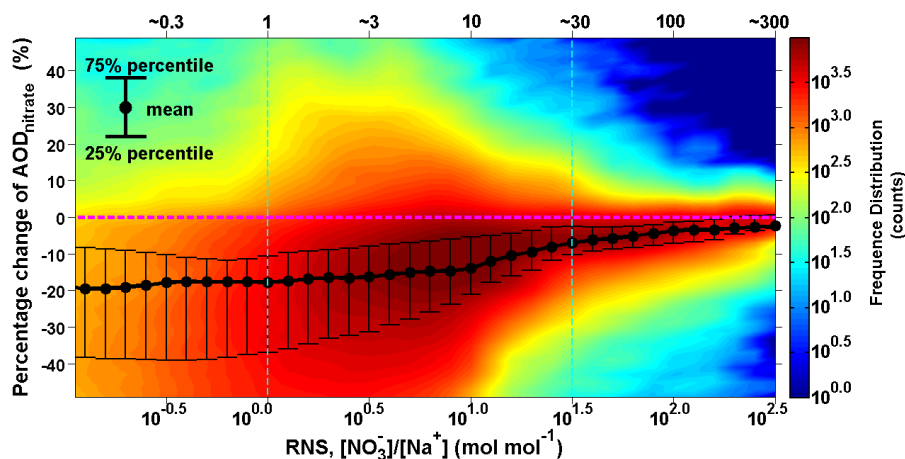


Fig. 6. Intensity of ‘re-distribution effect’ as a function of molar ratio between surface fine nitrate and total sodium (RNS) over European domain. The intensity of the re-distribution effect is calculated as the difference in percentage between AOD_{nitrate} and AOD_{nitrate}^* in the ‘Case_SeasaltOn’. The black dots indicate the mean values; the upper and lower error bars indicate the 75% and 25% percentile, respectively. The colour indicates the frequency distribution (i.e., how many counts) of the hourly model results over entire Europe domain during 16-20 September 2013. The coverage of model results between the two light blue dashed lines is ~70%.

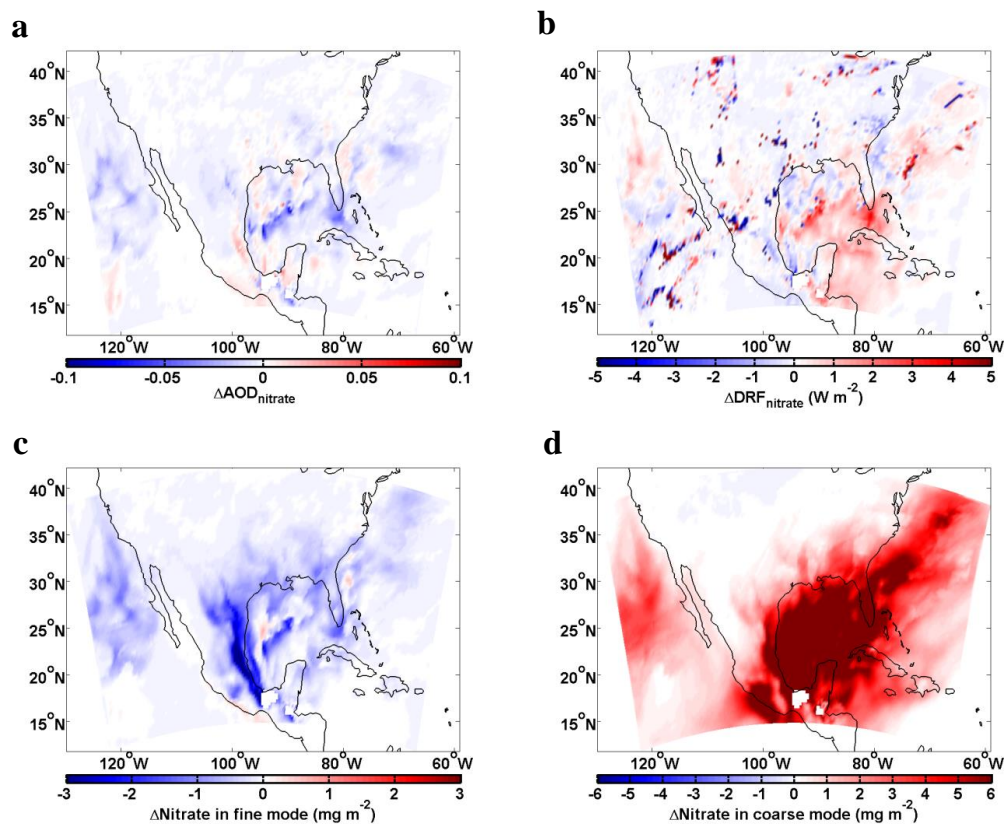


Fig. 7. Influence of sea-salt aerosol on the abundance and direct radiative forcing of nitrate (similar as Fig. 4). Differences ('Case_SeasaltOn' - 'Case_SeasaltOff') between simulations with and without sea-salt emission in aerosol optical depth ($\Delta AOD_{\text{nitrate}}$, **a**), direct radiative forcing ($\Delta DRF_{\text{nitrate}}$, **b**), and column loading of nitrate ($\Delta \text{Nitrate}$) for the fine (**c**) and coarse (**d**) mode particles. The modelled results showed here are averaged during daytime over North America domain, i.e., 16:00-22:00 (UTC) on 10-17 January 2015.

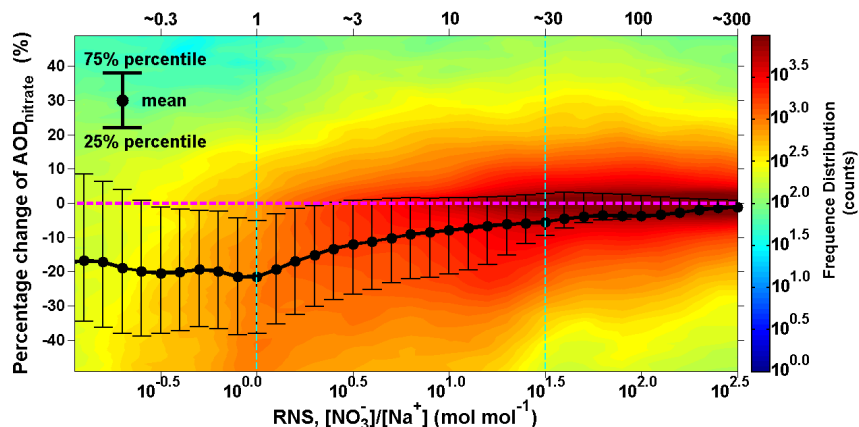


Fig. 8. Intensity of ‘re-distribution effect’ as a function of molar ratio between surface fine nitrate and total sodium (RNS) over North American domain, similar as Fig. 6. The intensity of ‘re-distribution effect’ is calculated as the difference in percentage between AOD_{nitrate} and AOD_{nitrate}^* in the ‘Case_SeasaltOn’. AOD_{nitrate}^* indicates the AOD_{nitrate} calculated by re-allocating nitrate mass into different size bins according to the normalized nitrate particle mass size distribution simulated in ‘Case_SeasaltOff’ (i.e., without ‘re-distribution effect’). The black dots indicate the mean values; the upper and lower error bars indicate the 75% and 25% percentile, respectively. The colour indicates the frequency distribution (i.e., how many counts) of the hourly model results over entire North America domain during 10-17 January 2015.

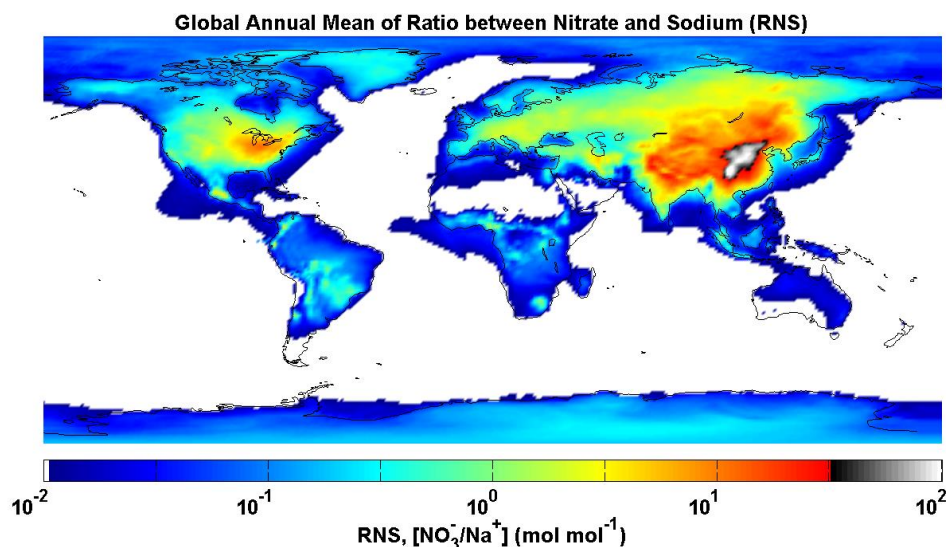


Fig. 9. The global distribution of annual mean RNS, simulated with the EMAC model. The regions with RNS smaller than 0.01, i.e., negligible particulate nitrate loading, are white.